Enhancing superconductivity in A_3C_{60} fullerides

Minjae Kim,[1,2,*] Yusuke Nomura,[1] Michel Ferrero,[1,2] Priyanka Seth,[2,3] Olivier Parcollet,[2,3] and Antoine Georges[1,2,4]

[1]*Centre de Physique Théorique, École Polytechnique, CNRS, Université Paris-Saclay, 91128 Palaiseau, France*

[2]*Collège de France, 11 place Marcelin Berthelot, 75005 Paris, France*

[3]*Institut de Physique Théorique (IPhT), CEA, CNRS, 91191 Gif-sur-Yvette, France*

[4]*Department of Quantum Matter Physics, University of Geneva, 24 Quai Ernest-Ansermet, 1211 Geneva 4, Switzerland*

(Received 18 June 2016; published 28 October 2016)

Motivated by the recent experimental report of a possible light-induced superconductivity in K_3C_{60} at high temperature [Mitrano *et al.*, Nature **530**, 451 (2016)], we investigate theoretical mechanisms for enhanced superconductivity in A_3C_{60} fullerenes. We find that an "interaction imbalance" corresponding to a smaller value of the Coulomb matrix element for two of the molecular orbitals in comparison to the third one, efficiently enhances superconductivity. Furthermore, we perform first-principle calculations of the changes in the electronic structure and in the screened Coulomb matrix elements of K_3C_{60}, brought in by the deformation associated with the pumped T_{1u} intramolecular mode. We find that an interaction imbalance is indeed induced, with a favorable sign and magnitude for superconductivity enhancement. The physical mechanism responsible for this enhancement consists of a stabilization of the intramolecular states containing a singlet pair, while preserving the orbital fluctuations allowing for a coherent interorbital delocalization of the pair. Other perturbations have also been considered and found to be detrimental to superconductivity. The light-induced deformation and ensuing interaction imbalance is shown to bring superconductivity further into the strong-coupling regime.

DOI: 10.1103/PhysRevB.94.155152

I. INTRODUCTION

Alkali-doped fullerenes A_3C_{60} (A = K, Rb, Cs) are a remarkable family of materials, which have the highest superconducting (SC) transition temperature among molecular superconductors ($T_c \sim 40$ K) [1,2]. Even though the gap symmetry is s wave, the mechanism of SC has been the subject of much debate [3–22]. Indeed, the narrow bandwidth ($W \sim 0.5$ eV), the intramolecular Coulomb interaction ($U \sim 0.6$ eV), and the typical frequency of the relevant intramolecular Jahn-Teller phonons ($\omega_{\rm ph} \sim 0.1$ eV) are comparable energy scales, which raises questions about the validity of conventional phonon-mediated SC mechanisms [3,5,23,24]. The experimental observation [25–35] of a Mott-insulating phase close to the SC phase in Cs_3C_{60} emphasizes the importance of strong electronic correlations for these materials and of their interplay with SC. [36–38]

Recently, a remarkable experiment [39] by Mitrano *et al.* reported a large enhancement in carrier mobility and the opening of an optical gap when exciting K_3C_{60} with a mid-infrared femto-second light pulse in the frequency range 80–200 meV (19–48 THz). These observations were interpreted as the signature of a light-induced SC at temperatures (up to $T \sim 100$ K) much higher than the equilibrium $T_c \sim 20$ K. This experiment raises a number of intriguing questions. On the theory side, one of the most pressing ones is whether there are indeed perturbations of the system which could lead to enhanced SC. And if so, whether such perturbations are likely to be induced by the mid-infrared excitation of Ref. [39]. Providing some answers to these two questions is the main purpose of this article.

In order to address these questions, we shall place ourselves within the theoretical framework reviewed in Ref. [3], which is one of the most successful ones at explaining the physical properties and SC of fullerenes. This approach focuses on the set of three near-Fermi level t_{1u} electronic states derived from the lowest unoccupied molecular orbitals. It furthermore recognizes two important ingredients for the physics of these materials. First, as pointed out early-on [24], the intramolecular Jahn-Teller phonons with H_g symmetry play a key role in the pairing. This leads to a reversal of the sign of the effective intramolecular exchange acting on the t_{1u} states (inverted Hund's coupling) [16,40]. Second, the intramolecular repulsion (Hubbard U) is comparable or larger than the bandwidth. This was shown [17] by Capone *et al.* to lead to a strong-coupling regime of the SC induced by the inverted Hund's coupling, near the Mott transition. This "inverted Hund's coupling" model [3] for the SC of fullerenes (IHSC) is introduced in more detail in Sec. II. Recently, an extensive first-principles study [19] by Nomura *et al.* has been successful at reproducing many properties of these materials and also validated the qualitative premises of the IHSC model.

The main finding of this article is that a perturbation which efficiently enhances SC indeed exists. This perturbation consists of an "interaction imbalance," in which the intramolecular Coulomb repulsion is larger by an amount $dU > 0$ in one of the t_{1u} orbitals, as compared to the two others. For example, at $dU/U \simeq 0.2$, the SC gap, order parameter, and critical temperature are increased by large amounts (a factor of 3.5, 1.6, and 1.8, respectively). We furthermore demonstrate, using first-principle calculations, that the THz pumping of the mid-infrared T_{1u} structural mode considered in Ref. [39] indeed leads to such a perturbation with a favorable sign $dU > 0$, and estimate the amplitude of the corresponding SC enhancement. Such an interaction imbalance was indeed discussed in Ref. [39], in relation also to previous work in which modulation of U by light excitation of organic materials was demonstrated [41]. However, the effect of this perturbation on SC was not investigated theoretically.

*garix.minjae.kim@gmail.com

Obviously the theoretical analysis presented here is an equilibrium one, while the observation made in Ref. [39] results from an out-of-equilibrium pump-probe experiment. As such, our work is a first step towards a full understanding of the experimental results. The main message is that the light-induced perturbation could indeed drive the system into a more strongly coupled SC regime.

II. INVERTED-J COUPLING MODEL AND SYMMETRY-BREAKING PERTURBATIONS

A. Inverted-Hund model and strongly correlated superconductivity

Let us briefly recall the key ingredients entering the IHSCmodel for the superconductivity of A_3C_{60} fullerenes, which will be used throughout this article (see Ref. [3] for a review). The model focuses on the three bands originating from the molecular t_{1u} states. The intramolecular Coulomb repulsion U associated with these states is comparable to their bandwidth $U/W \gtrsim 1$, so that the system is in the regime of strong correlations (consistent with the proximity of a Mott insulating state).

The H_g Jahn-Teller (JT) modes play an important role in the pairing and superconductivity. Their frequency is a significant fraction of the bandwidth ($\omega_{\rm ph}/W \sim 0.2$). Because of this, and of strong correlations, conventional Migdal-Eliashberg theory does not apply [42]. In the simplest version of the model, the phonon degrees of freedom are integrated out, leaving a purely electronic model for the three t_{1u} states. The distinctive feature of this model is that the effective Hund's coupling $J_{\rm inv}$ applying to these states has an inverted (antiferromagnetic) sign, in contrast to the conventional purely electronic Hund's coupling: $J_{\rm inv} = J_{\rm H} + J_{\rm JT} < 0$. The local (intramolecular) interactions applying to the t_{1u} states thus take the conventional Kanamori form:

$$H_{\rm int} = (U - 3J_{\rm inv})\frac{\hat{N}(\hat{N}-1)}{2} - 2J_{\rm inv}\vec{S}^2 - \frac{J_{\rm inv}}{2}\vec{L}^2 \qquad (1)$$

to which one should of course add the kinetic energy term (intermolecular hopping):

$$H_0 = \sum_{\mathbf{k}\sigma\alpha} \varepsilon_{\mathbf{k}} d^\dagger_{\mathbf{k}\sigma\alpha} d_{\mathbf{k}\sigma\alpha}. \qquad (2)$$

Here $\vec{S}$ and $\vec{L}$ are the spin and orbital angular momentum operators associated with the three orbitals, labeled by α (see, e.g., Ref. [43]).

For future reference, we note that the Kanamori interaction [Eq. (1)] can be rewritten [43] as $H_{\rm int} = H_{nn} + H_{\rm sf} + H_{\rm ph}$, in which H_{nn} involves only density-density interactions, $H_{\rm sf}$ is a spin-flip term, and the "pair-hopping" term $H_{\rm ph}$. $H_{\rm ph}$ transfers a singlet pair from one orbital to another one, namely

$$\begin{aligned} H_{nn} &= U\sum_{\alpha} \hat{n}_{\alpha,\uparrow}\hat{n}_{\alpha,\downarrow} \\ &\quad + (U - 2J_{\rm inv})\sum_{\alpha\neq\beta} \hat{n}_{\alpha,\uparrow}\hat{n}_{\beta,\downarrow} \\ &\quad + (U - 3J_{\rm inv})\sum_{\alpha<\beta,\sigma} \hat{n}_{\alpha,\sigma}\hat{n}_{\beta,\sigma}, \end{aligned}$$

$$\begin{aligned} H_{\rm sf} &= -J_{\rm inv}\sum_{\alpha\neq\beta} d^\dagger_{\alpha,\uparrow} d_{\alpha,\downarrow} d^\dagger_{\beta,\downarrow} d_{\beta,\uparrow}, \\ H_{\rm ph} &= J_{\rm inv}\sum_{\alpha\neq\beta} d^\dagger_{\alpha,\uparrow} d^\dagger_{\alpha,\downarrow} d_{\beta,\downarrow} d_{\beta,\uparrow}. \end{aligned} \qquad (3)$$

The rationale for $J_{\rm inv} < 0$ is that the JT modes dynamically lift the degeneracy of the three states, hence favoring the $S = 1/2, L = 1$ local configuration when three electrons occupy the t_{1u} molecular orbital (half-filled shell, as appropriate for A_3C_{60}). This is in contrast to the $S = 3/2, L = 0$ configuration favored by the electronic Hund's coupling. The sixfold degenerate $S = 1/2, L = 1$ configuration basically consists of one singlet pair occupying any of the three orbitals, and a third lone electron in one of the two remaining ones (see Sec. V A). Through the intramolecular pair-hopping term $H_{\rm ph}$, this pair is delocalized between any of the three orbitals, and these orbital fluctuations promote SC [19,22].

The basic reason for which SC is driven into the strong-coupling regime (hence leading to high T_c) in this model is the following [3,17]. As the Mott transition is approached, charge fluctuations are suppressed and the quasiparticle bandwidth is renormalized by the Brinkman-Rice phenomenon [44] down to ZW with Z the quasiparticle spectral weight. In contrast, the $J_{\rm inv}$ interaction does not couple to the charge sector, but only to the spin and orbital sectors, and hence this interaction is basically unrenormalized. As a result, the effective attractive coupling $J_{\rm inv}/ZW$ becomes large and the SC enters the strong-coupling regime. As U/W is increased from the weak-coupling regime, the SC gap, T_c, and the SC order parameter increase. The latter decreases again as the Mott transition is approached, following a domelike behavior (see Fig. 10 in the Appendix).

Simplified as it may be, several observations provide a justification to the IHSC model as a minimal model for the SC of A_3C_{60} fullerenes. The spin gap corresponding to the transition between low-spin $S = 1/2, L = 1$ and high-spin $S = 3/2, L = 0$ configurations ($\sim 5J_{\rm inv} \sim 0.1$ eV, see Sec. V A) is indeed observed in nuclear magnetic resonance experiments [45,46]. Also, a recent first-principle investigation [19] treating electronic correlations according to (1) but explicitly taking into account JT phonon modes turns out to quantitatively describe the phase diagram of A_3C_{60} materials as a function of unit-cell volume.

B. Symmetry-breaking perturbations: U imbalance and crystal-field splitting

Our strategy in this article is to consider perturbations of the Hamiltonian [Eqs. (1) and (2)] and to identify which perturbations can lead to an enhancement of superconductivity. We consider specifically two kinds of perturbations, of which both break the symmetry between t_{1u} orbitals.

The first one ("U imbalance") is a perturbation that modifies the intramolecular Coulomb energy U for two of the orbitals (conventionally chosen to be x and y) as compared to the third one:

$$H_{dU} = -dU(\hat{n}_{x,\uparrow}\hat{n}_{x,\downarrow} + \hat{n}_{y,\uparrow}\hat{n}_{y,\downarrow}). \qquad (4)$$

For $dU > 0$, the Coulomb energy becomes smaller for these two orbitals, while it becomes larger for $dU < 0$. As we shall

see, these two signs of the perturbation lead to very different effects on SC.

The second perturbation ("crystal field") is a splitting between the molecular energy levels of the x,y orbitals and that of the z orbital, hence lifting the degeneracy of the t_{1u} triplet at the one-electron level:

$$H_{\rm CF} = h_{\rm CF}\,(\hat{n}_x + \hat{n}_y). \tag{5}$$

In contrast to the U-imbalance case, this commutes with L_z: $[H_{\rm CF}, L_z] = 0$. This perturbation was also considered recently in Ref. [47]. As shown there (see also Appendix A 2), $h_{\rm CF} > 0$ and $h_{\rm CF} < 0$ are equivalent in the presence of particle-hole symmetry.

In Sec. IV we motivate the study of these two perturbations above from first-principle studies of K_3C_{60} subject to a THz pump exciting the T_{1u} structural mode. The reader is thus directed to this section for physical motivations of these perturbations.

C. Methods and observables

We solve the IHSC model in the presence of the perturbations above using dynamical mean-field theory (DMFT, for a review see, e.g., Ref. [48]). For simplicity, the noninteracting density of states (DOS) associated with the dispersion $\varepsilon_{\mathbf{k}}$ is chosen to be a semicircular with width W. This corresponds to a Bethe lattice in the limit of infinite coordination, for which DMFT becomes exact.

In order to solve the model in the superconducting phase, we introduce a Nambu spinor $\Psi_\alpha^\dagger \equiv (d_{\alpha\uparrow}^\dagger, d_{\alpha\downarrow})$ for each orbital $\alpha = x,y,z$. For the chosen semicircular DOS, the dynamical mean-field $\mathcal{G}$ (Weiss function) [48] entering the impurity model is then given by the self-consistency condition:

$$\hat{\mathcal{G}}_\alpha^{-1}(i\omega_n) = i\omega_n \mathbf{1} + \mu\tau_z - \left(\frac{W}{4}\right)^2 \tau_z \hat{G}_\alpha(i\omega_n)\tau_z. \tag{6}$$

In this expression we have used Nambu matrix notations (with τ_z the Pauli matrix), $\hat{G}_\alpha(\tau) \equiv -\langle T\,\Psi_\alpha(\tau)\Psi_\alpha^\dagger(0)\rangle$ denotes the local (on-site) Green's function in matrix form, and the ω_n are Matsubara frequencies. The chemical potential μ is adjusted to ensure an occupancy of three electrons per site.

We solved the DMFT quantum impurity problem using the hybridization expansion continuous-time quantum Monte Carlo (CTQMC) solver [49], as implemented in the TRIQS library [50,51]. It should be noted that, in order to properly sample the SC phase, four-operators insertions are essential in Monte Carlo updates [52,53].

In order to characterize the SC phase, we focus in particular on the following observables.

(1) The orbitally resolved pairing amplitude $P_{\rm sc}^\alpha$ and total SC order parameter $P_{\rm sc}$ (summed over all orbitals), obtained from the off-diagonal component of the Green's function in Nambu matrix form:

$$P_{\rm sc}^\alpha = G_\alpha^{12}(\tau = 0^+), \quad P_{\rm sc} = \sum_{\alpha=x,y,z} G_\alpha^{12}(\tau = 0^+). \tag{7}$$

(2) The quasiparticle spectral weight for each orbital Z_α, defined from the diagonal component of the retarded self-energy:

$$Z_\alpha = \left[1 - \frac{\partial {\rm Re}\,\Sigma_{{\rm ret},\alpha}^{11}}{\partial\omega}\bigg|_{\omega=0}\right]^{-1}. \tag{8}$$

In practice, this can be accurately approximated at low temperature from the first Matsubara frequency:

$$Z_\alpha \simeq \left[1 - \frac{{\rm Im}\,\Sigma_\alpha^{11}(i\omega_0)}{\omega_0}\right]^{-1}. \tag{9}$$

(3) From the low-frequency expansion of the Nambu Green's function, we see that the dispersion of the α-orbital quasiparticles in the SC state read $\omega_\pm^\alpha(\mathbf{k}) = \pm Z_\alpha\sqrt{(\varepsilon_{\mathbf{k}} - \mu)^2 + [\Sigma_\alpha^{12}(0)]^2}$. Hence the SC gap for orbital α is given by

$$\Delta_\alpha = Z_\alpha \Sigma_\alpha^{12}(0) \simeq Z_\alpha \Sigma_\alpha^{12}(i\omega_0). \tag{10}$$

(4) The SC critical temperature T_c was estimated by stabilizing a SC solution for several different temperatures, and fitting the corresponding temperature dependence of the order parameter to a mean-field form $P_{\rm sc}(T) = C\sqrt{T_c - T}$ for three temperatures closest to the boundary of the SC phase.

The parameters in all the following will be chosen in accordance with values determined in previous work [54,55] as appropriate for the description of K_3C_{60}. Unless stated otherwise, we take $U = W$ and $J_{\rm inv} = -0.04W$. Most of the results below are displayed at the lowest temperature we have studied in the SC phase, namely $T = 0.005W$. For K_3C_{60}, the t_{1u} bandwidth is of order $W \simeq 0.50$ eV and hence $U = 0.50$ eV, $J_{\rm inv} = -20$ meV.

III. RESULTS

In this section we present our main findings regarding the effect of the above perturbations on superconductivity.

A. Imbalanced Coulomb interaction

Figure 1(a) displays the superconducting order parameter and orbitally resolved gaps as a function of the imbalance dU/U. A negative imbalance $dU < 0$ (i.e., having a larger Coulomb repulsion on two orbitals as compared to the third

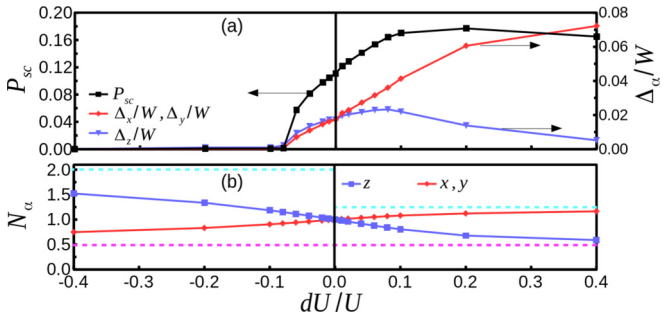

FIG. 1. (a) Total superconducting (SC) order parameter $P_{\rm sc}$ and orbitally resolved SC gaps Δ_α/W as a function of the interaction imbalance dU/U [as defined in Eq. (4)]. (b) Orbital occupancies as a function of dU/U. Dashed lines indicate asymptotic values of the orbital occupancies discussed in the text, for $dU < 0$ and $dU > 0$, respectively.

one) is detrimental to SC. In contrast, a positive imbalance (smaller repulsion on two of the orbitals) leads to a remarkable enhancement of superconductivity. The largest enhancement of the total SC order parameter $P_{\rm sc}$ is found at $dU/U \simeq 0.2$, at which $P_{\rm sc}$ is enhanced by a factor of $\sim$1.6 over its value for the degenerate case ($dU = 0$), while the SC gap for the x,y orbitals is enhanced by a factor of $\sim$3.5 and the critical temperature by a factor of $\sim$1.8 (see Fig. 3 for summary) !

We note that such a large enhancement cannot be obtained by an overall increase of U/W for all of the orbitals, which would correspond to an isotropic volume control of the material [31]. Indeed, the chosen value $U/W = 1$ is already quite close to $U/W \simeq 1.2$ at which $P_{\rm sc}$ is maximum, and only a very small enhancement of $P_{\rm sc}$ can be obtained by increasing U/W (see also Fig. 3).

Indeed, orbital differentiation is crucial to the effect, as seen from the orbitally resolved gaps displayed in Fig. 1(a) and from the orbital occupancies in Fig. 1(b). Upon increasing dU/U, the SC gap associated with the two orbitals (x,y) having a smaller U increases monotonically up to $\sim 0.07W$ at $dU/U = 0.40$. In contrast, Δ_z has a maximum and quickly decreases to a small value. Correspondingly, the occupancy of the x,y orbitals increases and that of the z orbital decreases, reaching limiting values at large dU/U. These limiting values are easily understood qualitatively for a simplified interaction which would contain only density-density terms. For $U_{zz} \gg U_{xx} = U_{yy}$, a double occupancy is created in, say, the x orbital, while the third electron is shared equally between y and z—an equally probable configuration having reversed roles of x and y which are identical by symmetry [see Fig. 5(b)]. Hence in this case $N_x = N_y = 1/2(2 + 1/2) = 1.25$ and $N_z = 1/2$. The limiting values we observe in our calculation for the full interaction [Eq. (1)] are somewhat reduced from these ones by the pair-hopping term and charge fluctuations (Fig. 1, bottom panel).

These considerations suggest that the increased weight of configurations having a double occupancy in the x or y orbital is crucial to the enhancement of the SC. Section V addresses the physical mechanism underlying this effect in more details. We shall see there that the formation of a spin-singlet pair is indeed crucial, but that an additional requirement is that these pairs can delocalize and become mobile through orbital fluctuations and pair hopping. This is indeed the case for $dU > 0$, because the pair forms in either of the two degenerate, symmetry-equivalent x,y orbitals.

This also explains why a negative dU is detrimental to SC. In this case, formation of a pair is favored in the z orbital, as seen from the increase of N_z in Fig. 1. Since a single orbital is involved, the pair is localized and cannot benefit from pair hopping between orbitals. Noteworthy is that SC is completely suppressed (at $dU/U \simeq -0.1$) significantly before complete orbital polarization is reached [corresponding to $N_z = 2, N_{x,y} = 1/2$, as indicated by dashed lines in Fig. 1(b)].

B. Crystal field

Figure 2 displays our results in the presence of a crystal-field splitting, Eq. (5). The results are displayed for $h_{\rm CF} > 0$, since $h_{\rm CF} < 0$ is equivalent by symmetry (Appendix A 2). We see

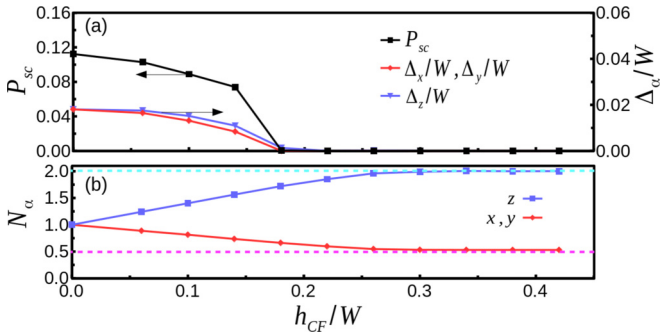

FIG. 2. (a) SC order parameter $P_{\rm sc}$ and SC gaps Δ_α/W as a function of the crystal-field $h_{\rm CF}/W$ as defined in Eq. (5). (b) Orbital occupancies as a function of $h_{\rm CF}/W$. Dashed lines indicate full orbital polarization into the z-orbital singlet configuration (see text).

that this perturbation is detrimental to SC, in agreement with the recent findings of Ref. [47]. Although the perturbation of $h_{\rm CF} > 0$ favors the formation of a doubly occupied pair in the z orbital, orbital fluctuations are suppressed and the pair cannot delocalize as for $dU < 0$. We note however that, in contrast to the $dU < 0$ case, complete suppression of SC occurs only close to full orbital polarization $N_z = 2, N_{x,y} = 0.5$. Hence, one can say that SC is more robust in the presence of a crystal field than in the presence of an interaction imbalance with $dU < 0$. We discuss this difference in more detail in Sec. V

C. Summary and comparison of different perturbations

Figure 3 provides a summary of some of our results for the key observables (SC order parameter, gaps, and T_c) and allows for a comparison between different cases, with reference to the $U/W = 1$ degenerate case which serves as a reference point.

(1) The results displayed for $U/W = 1.2$ in the absence of any perturbation (degenerate case) demonstrate that only a very modest enhancement of T_c (by factor of $\sim$1.1) is obtained from a global increase of U/W corresponding to a uniform compression of the system, as stated above.

(2) At the largest enhancement of the $P_{\rm sc}$, $dU/U = 0.2$ (with $h_{\rm CF} = 0$), the remarkably large enhancements noted above are found, by a factor $\sim$1.6 for the total order parameter, $\sim$1.8 for T_c and $\sim$3.5 for the gap $\Delta_{x,y}$.

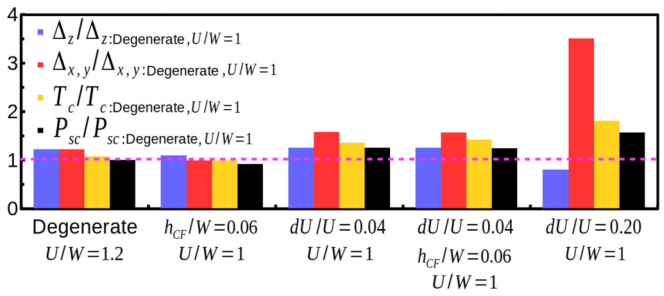

FIG. 3. Summary of key results under various perturbations: SC gaps, SC critical temperature T_c, and SC order parameter $P_{\rm sc}$, all normalized to their corresponding values for $U/W = 1$ in the degenerate case $dU = h_{\rm CF} = 0$.

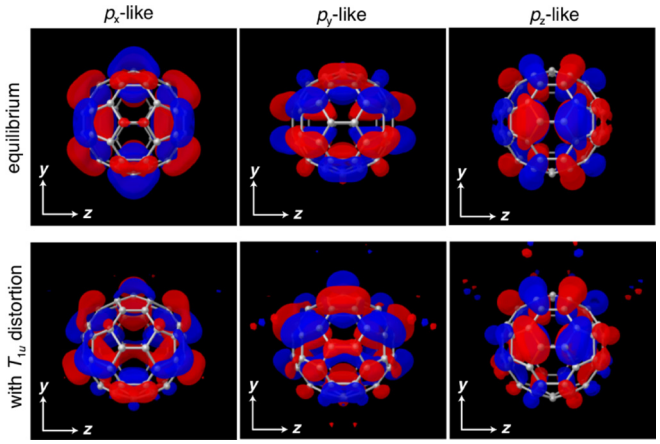

FIG. 4. Top row: t_{1u} Wannier functions for K_3C_{60} in the equilibrium structure. Bottom row: Wannier functions in the transient structure obtained by selectively exciting the $T_{1u}(4)$ phonon mode along the y axis, at a maximum amplitude (corresponding to a 1/4 cycle) of 2.0 (Å$\sqrt{\text{amu}}$)—see Ref. [39]. Note that only the p_z-like orbital has a preserved nodal surface in that case (corresponding to the xy plane), leading to a larger value of U for that orbital. Only a single molecule is shown for visibility. The red (blue) color corresponds to positive (negative) isosurfaces of the Wannier function. In the transient structure p_x-like and p_y-like orbitals (see text) do not have nodes but remain equivalent by symmetry (see Fig. 13).

(3) We have also displayed results for a more modest imbalance $dU/U = 0.04$. As explained in Sec. IV, this is our estimate for a realistic value of dU/U induced by THz pumping in the experiments of Mitrano *et al.* [39]. Remarkably, a quite sizable enhancement of SC by a factor of ∼1.35 for T_c is found there, despite the small value of dU/U. As also shown in Fig. 3, this enhancement is not much affected by a small crystal field $h_{\text{CF}}/W \simeq 0.06$ (enhancement of T_c by factor of ∼1.41 with respect to degenerate case) which may also be induced by the THz pump (Sec. IV).

(4) In the case of $dU > 0$ for which T_c is enhanced, the SC gap is strongly orbital dependent, with $\Delta_{x,y}$ larger than Δ_z. For example, for $dU/U = 0.2$, $\Delta_{x,y}$ is enhanced by a factor of ∼3.5 with respect to the degenerate case, while Δ_z is reduced by ∼0.7. This orbital dependence of the SC gap is reflected in the density of states displayed in Fig. 12(d). Time-resolved tunneling spectroscopy may provide a probe of this two-gap structure, a wide gap in the x and y orbitals, and a narrow gap in the z orbital.

IV. TERA-HERTZ EXCITATION AND U IMBALANCE

In this section we make contact with the experiment of Mitrano *et al.* [39] by estimating the typical magnitude of the perturbations dU/U and h_{CF}/W induced by the mid-infrared optical pulse employed by these authors. It was proposed in Ref. [39] that this optical pulse excites the $T_{1u}(4)$ intramolecular vibrational mode of the C_{60} molecule, and a typical value of 2.0 Å$\sqrt{\text{amu}}$ was quoted for the normal coordinate excited amplitude of this mode.[1] In turn, the perturbation modifies the electronic structure of the t_{1u} states.

We have calculated the three Wannier functions associated with these electronic states in both the unperturbed equilibrium structure, and in the perturbed structure corresponding to the $T_{1u}(4)$ vibrational mode at the above quoted amplitude (i.e., for a quarter cycle of the pulse). The results are displayed in Fig. 4, for a polarization of the pulse conventionally chosen along the y axis. As expected, in the equilibrium structure (upper panel), we have three (degenerate) orbitals p_x, p_y, and p_z having nodal surfaces in the yz, zx, and xy plane, respectively. In the deformed structure (lower panel), the C-C bonds are distorted along the x direction with odd symmetry along the y direction. As a result, only the node in the xy plane is preserved, corresponding to a p_z-like orbital displayed on the lower right of Fig. 4. In contrast, as clear from Fig. 4, the two other nodal planes (zx and yz) are absent in the perturbed structure, corresponding to two Wannier orbitals that we still denote "p_x-like" and "p_y-like." While the inversion symmetry along the y axis is broken by the perturbation, inversion symmetry along the x and z axis is preserved, and the two orbitals p_x and p_y are still degenerate (see Fig. 13).

In order to evaluate the matrix elements of the screened Coulomb interaction in both the equilibrium and perturbed structure, we have used the constrained-RPA (cRPA) *ab initio* method [56]. In a nutshell, this method computes the effect of screening in the random-phase approximation (RPA/GW), including all particle-hole excitations except those for which both the initial and final states belong to the "target manifold" of t_{1u} states retained in the low-energy many-body interaction Hamiltonian [Eq. (1)]. Matrix elements of this constrained screened interaction between the above Wannier states are

[1]The C–C bond lengths in the presence of this amplitude of distortion (2.0 Å $\sqrt{(\text{amu})}$) are 1.065 Å (shorter bond) to 1.7460 Å (longer bond). In the equilibrium structure of K_3C_{60}, the average C–C bond length is 1.426 Å (1.397–1.437 Å).

TABLE I. Coulomb interaction matrix elements, as evaluated from cRPA, in the equilibrium structure and in the presence of the T_{1u} excitation. The screened values correspond to the coupling constants acting on the low-energy t_{1u} electronic states. Values of the bare Coulomb interaction matrix elements without screening are also presented. U and J_{H} are on-site (local) couplings, while V is the intersite (nearest-neighbor) Coulomb interaction. Calculations including both the T_{1u} and H_g distortions were also performed (not shown), leading only to minor changes in the results for only T_{1u} distortion case

	$U_{x,y}$ (eV)	U_z (eV)	$J_{\text{H}:xz,yz}$ (eV)	$J_{\text{H}:xy}$ (eV)	V (eV)
Equilibrium (cRPA)	0.70	0.70	0.033	0.033	0.21
With T_{1u} (cRPA)	0.79	0.81	0.041	0.036	0.23
Equilibrium (unscreened)	3.23	3.23	0.096	0.096	1.36
With T_{1u} (unscreened)	3.47	3.58	0.14	0.12	1.36

then calculated. The results are displayed in Table I, calling for the following observations.

(1) Overall, the effective intramolecular repulsion $U_{\rm eff}$ (which can be approximately estimated as $U - V$ with U the local component and V the nearest-neighbor one, see Fig. 3 in Ref. [19]) is increased by the $T_{1u}(4)$ distortion for all orbitals, by a factor up to $\sim$1.2. This is because the $T_{1u}(4)$ distortion reduces the average distance between electrons in the t_{1u} states. Note however that, as discussed above, this overall increase of the effective U does not lead to a significant enhancement of SC.

(2) The screened Coulomb interaction for the node-preserving p_z orbital ($U_z = 0.81$ eV, $U_z - V = 0.58$ eV) is larger than for the p_x, p_y orbitals ($U_{x,y} = 0.79$ eV, $U_{x,y} - V = 0.56$ eV). This corresponds to a positive value of the interaction imbalance of order $dU/U \simeq 0.04$ (considering the effective interaction $U - V$). The physical reason for this is twofold. First, as shown in Fig. 4, the p_z orbital in the distorted structure displays an asymmetric charge distribution, with lobes of quite different sizes for $y > 0$ as compared to $y < 0$ because of the y-inversion symmetry breaking. As a result, there is an enhanced probability of having two electrons closer to one another (for $y > 0$ in Fig. 4) in this orbital. In contrast, the suppression of the nodal surfaces for the x, y orbitals leads to a more uniform charge distribution, so that this asymmetric contraction is moderate for those orbitals. Note that, in Ref. [39], a calculation using a Hückel model for the molecular orbitals and simple electrostatics led to the opposite conclusion $dU < 0$. However, the reshaping of the molecular orbitals by the distortion (as well as screening) was not fully taken into account.

(3) We have also calculated the value of the *electronic* (ferromagnetic) Hund's coupling in both the equilibrium and distorted structure. A small increase is found (0.008 and 0.003 eV for x, y and z, respectively). The effect of this on the effective inverted Hund's coupling would require an *ab initio* evaluation of the change in the coupling to the Jahn-Teller phonons, which we have not attempted here. Hence, for simplicity, we kept $J_{\rm inv}$ constant in our study.

So far we have considered the direct effect of the pumped $T_{1u}(4)$ mode. In Ref. [39] it was suggested that this mode could also induce a deformation of other structural modes through a nonlinear coupling ("nonlinear phononics," see Refs. [57,58]). For example, a coupling of the form $Q^2_{T_{1u}} Q_{H_g}$ to a Raman-active H_g mode was considered, and its effect on the electronic structure of the t_{1u} states calculated [39]. The resulting crystal-field splitting in the perturbed structure [with both $T_{1u}(4)$ and H_g perturbation] was found to be $h_{\rm CF}/W \simeq 0.06$. This is the motivation for also including this perturbation in the model calculations reported above. We have found that a crystal field of this magnitude does not spoil the SC enhancement resulting from the $dU/U \simeq +0.04$ imbalance.

V. MECHANISM OF SUPERCONDUCTIVITY ENHANCEMENT

In this section we discuss in some detail the mechanism leading to SC enhancement or suppression by the two perturbations considered in this article.

A. Molecular eigenstates and histograms

First, we analyze the eigenstates (multiplets) of the interaction Hamiltonian (1) for an isolated molecule, and how they are modified by the perturbations. This analysis is summarized in Fig. 5.

Consider first the inverted Hund's coupling interaction with density-density terms only [i.e., omitting the pair-hopping and spin-exchange terms contained in Eq. (3)]. As displayed in Fig. 5(a), the ground state is the (210) state made of a singlet pair in one of the orbitals, a single electron in another orbital, and an empty orbital. The excited states all have one electron in each orbital, in either the $(11\bar{1})$ with one spin-flip or (111) spin-parallel configurations. These states are separated by $2|J_{\rm inv}|$ and $4|J_{\rm inv}|$ from the ground state, respectively.

For the full Kanamori Hamiltonian [Eq. (1)] involving pair-hopping and spin-flip terms, these multiplets rearrange into eigenstates of S and L, as indicated by the arrows in Fig. 5(a). The sixfold degenerate ground state has $(S = 1/2, L = 1)$: it can be viewed as a resonant superposition of the different (210) states with a singlet pair delocalized between the different orbitals. The presence of a singlet pair in the ground state and its coherent delocalization over orbitals through the pair-hopping term is key to the SC found in the IHSC model. This enhancement of SC by pair tunneling between different orbitals was considered in Refs. [59,60], and is sometimes referred to as the Suhl-Kondo mechanism. Excited multiplets have $(S = 1/2, L = 2)$ and $(S = 3/2, L = 0)$ and are separated from the ground-state manifold by $2|J_{\rm inv}|$ and $5|J_{\rm inv}|$, respectively.

In Figs. 5(b)–5(d) we display the effect of the three perturbations $dU > 0$, $dU < 0$, and $h_{\rm CF}$, respectively, focusing for simplicity on a density-density interaction only. The $dU > 0$ perturbation [Fig. 5(b)] affects the (210) multiplets only. States with the spin-singlet pair in the z orbital are unaffected, while those with the pair in the x or y orbital are energetically stabilized, by an amount dU. Hence, $dU > 0$ leads to a relative stabilization of (210) states with a pair in the x or y orbital, as compared to the (111) and $(11\bar{1})$ states. This is a key ingredient for the promotion of SC by the $dU > 0$ perturbation.

In contrast for $dU < 0$ [Fig. 5(c)], the states with a pair in the x or y orbital are lifted up in energy, while the molecular ground state with a pair in the z orbital is unaffected. This corresponds to a relative destabilization of the (210) multiplet as compared to the (111) and $(11\bar{1})$ ones. Furthermore, because the pair is now localized in a single orbital, the pair-hopping term is ineffective. Both factors lead to a suppression of SC.

This analysis is based on the t_{1u} many-body eigenstates of an isolated molecule, as described by [Eq. (1)]. In order to confirm its relevance to the full solid in the presence of intermolecular hopping, we have calculated the probability for a given state to be visited during the Monte Carlo sampling performed in the full DMFT calculation [61]. This is displayed in Fig. 6. Figure 6(a) demonstrates that indeed the (210) states are stabilized by the $dU > 0$ perturbation, and destabilized for $dU < 0$, relative to the (111) or $(11\bar{1})$ states.

Figure 5(d) displays the energy levels in the presence of a crystal field with $h_{\rm CF}$. The different components of the (210) ground-state manifold are lifted up in energy by $h_{\rm CF}$, $2h_{\rm CF}$, and $3h_{\rm CF}$ depending on whether the z orbital is doubly

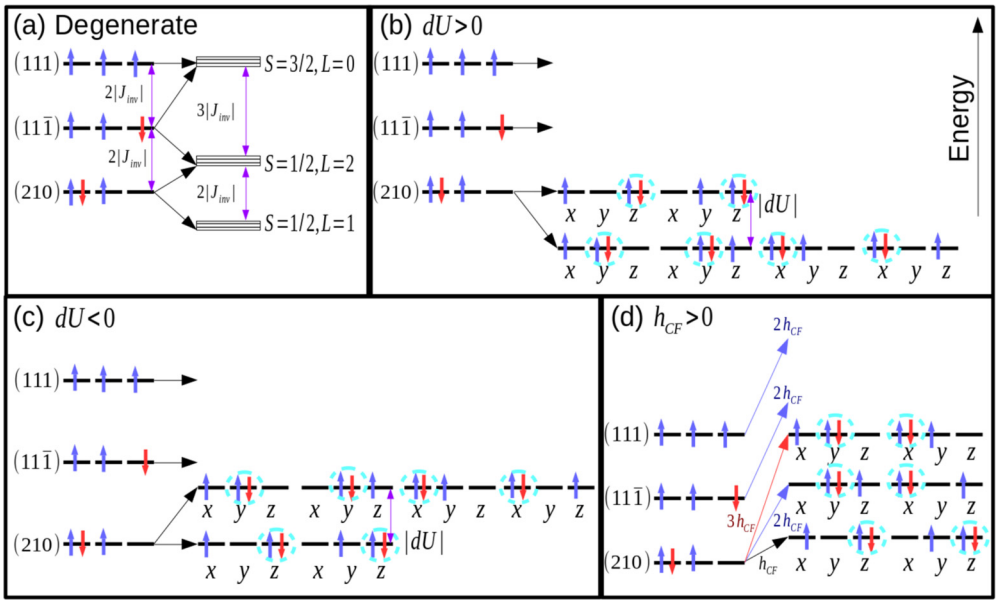

FIG. 5. Multiplets of eigenstates for an isolated molecular site, for a half-filled t_{1u} shell occupied by three electrons. (a) In the absence of any perturbation and when only density-density interactions are considered, the (210), (11$\bar{1}$), and (111) states are eigenstates. For the Kanamori Hamiltonian (1) involving pair-hopping and spin-flip terms, these states reorganize into ($S = 3/2, L = 0$), ($S = 1/2, L = 2$), and ($S = 1/2, L = 1$) multiplets, as indicated by the arrows. (b), (c), and (d) Eigenstates for a density-density interaction Hamiltonian [H_{nn} in Eq. (3)], in the presence of the perturbations $dU > 0$, $dU < 0$ [Eq. (4)], and h_{CF} [Eq. (5)], respectively.

occupied, singly occupied, or empty, respectively. Excited states (111) and (11$\bar{1}$) are lifted up by $2h_{CF}$. As a result, the energy difference between the molecular (210) ground state, which was $2|J_{inv}|$ in the absence of the perturbation, is now increased to $2|J_{inv}| + h_{CF}$. This corresponds to a relative stabilization of the (210) multiplet, as also demonstrated for the full calculation by the statistical weights displayed in Fig. 6(b). We have seen, however, that SC is suppressed by the crystal-field perturbation. Hence, stabilization of the (210) manifold is not a sufficient condition for the promotion of SC: pair delocalization through orbital fluctuations is crucial, and we now analyze this in more detail.

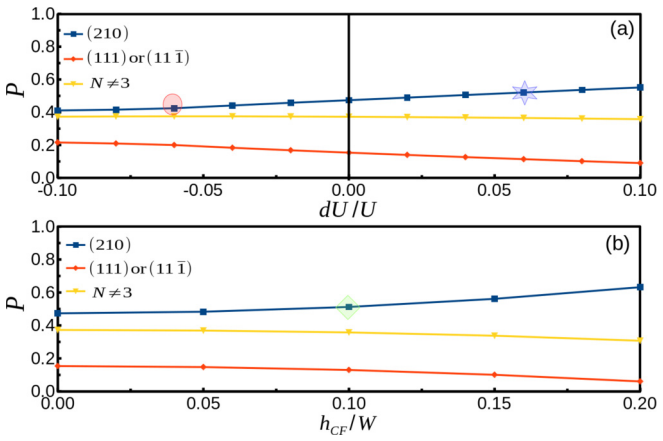

FIG. 6. Statistical weights of the (210), (111), or (11$\bar{1}$) states in the presence of (a) an interaction imbalance and (b) a crystal-field perturbation, as obtained from DMFT. Data indicated by circle (red), star (blue), and square (green) are analyzed in detail in Fig. 8.

B. Key role of orbital fluctuations

Orbital fluctuations within the multiplet of (210) states promote superconductivity. The pair-hopping term [Eq. (3)] induces the formation of an intramolecular resonant state with ($S = 1/2, L = 1$). In the degenerate case, the corresponding singlet pair can live in any of the three orbitals, as illustrated in Fig. 7(a). The other panels in this figure illustrate the fact that orbital fluctuations allowing the singlet pair to delocalize between different orbitals are still possible for $dU > 0$, but are hampered for both $dU < 0$ and in the presence of a crystal field.

Figure 8 presents a more in-depth analysis of the computed statistical weights of states forming the (210) manifold, for three representative cases of $dU > 0$, $dU < 0$, and crystal

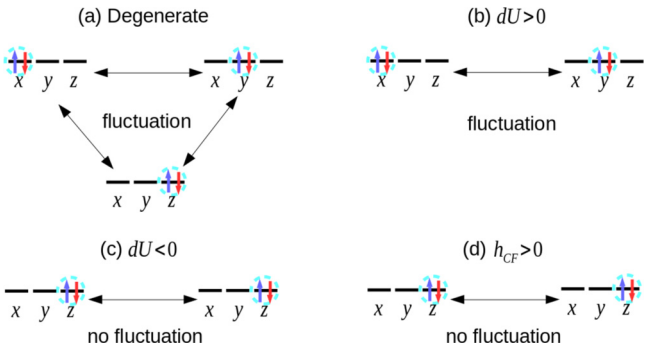

FIG. 7. This figure illustrates the key role of ground-state orbital fluctuations in promoting SC. These fluctuations are present in the unperturbed degenerate case (a), are preserved for $dU > 0$ (b), while they are suppressed for $dU < 0$ (c), or the presence of h_{CF} (d). Note that, for clarity, only the location of the pair in the ground state is displayed in this figure—the third lone electron has been omitted.

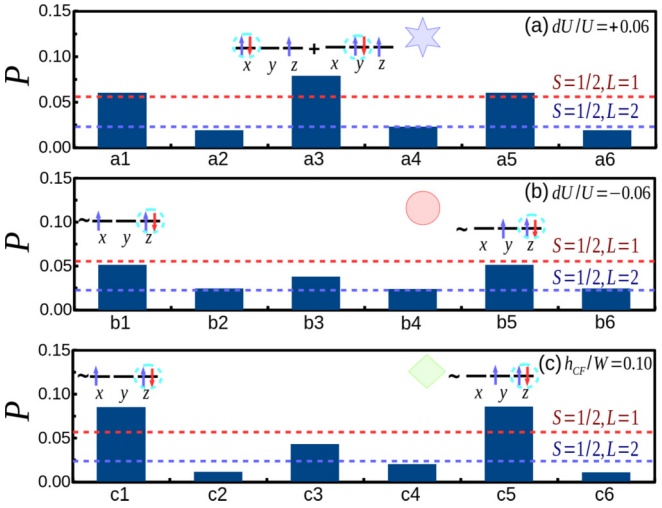

FIG. 8. Histogram of statistical weights for (a) $dU/U = 0.06$, (b) $dU/U = -0.06$, and (c) $h_{\rm CF}/W = 0.10$. The most dominant multiplets are plotted in each case. See Fig. 14 for the precise definition of eigenstates a1–a6, b1–b6, and c1–c6.

field. This figure complements Fig. 6 in which only the global weight of the (210) multiplet was presented. Here we display the weights obtained by measuring statistical weights of each eigenstate of the Hamiltonian in the (210) manifold (detailed in Appendix A 6). We observe that:

(1) For $dU > 0$ [Fig. 8(a)], the state which is a resonant superposition of a singlet pair in the x and y orbitals (plus a lone electron in the z orbital) has the largest statistical weight. Its weight is even larger than that of the $(S = 1/2, L = 1)$ states in the degenerate case. This fully confirms that the enhancement of SC observed in this case originates from the stabilization of states involving a spin-singlet pair together while preserving orbital fluctuations.

(2) For $dU < 0$ [Fig. 8(b)], the dominant states are those with a pair in the z orbital only, hence suppressing orbital fluctuations. Also the corresponding weight is reduced as compared to that of the $(S = 1/2, L = 1)$ states in the degenerate case. This confirms that the suppression of SC even when orbital polarization is incomplete originates from both the destabilization of singlet pair configurations and in the suppression of orbital fluctuations.

(3) In the presence of a crystal field [Fig. 8(c)], we have a mixed situation: the weight of states having a spin-singlet pair is enhanced [by a factor ∼1.75 in Fig. 8(c)] as compared to that of the $(S = 1/2, L = 1)$ multiplet in the degenerate case. However, this increased weight corresponds to states with a pair in the z orbital only, for which orbital fluctuations are suppressed. As a result, the SC phase is resilient as long as the orbital polarization is incomplete and is finally suppressed only when $h_{\rm CF}/W$ is large enough to yield full orbital polarization and complete quenching of orbital fluctuations, as shown in Fig. 2.

C. Driving superconductivity into the strong-coupling regime

Finally, we demonstrate in this section that turning on the imbalance perturbation $dU > 0$ increases the effective pairing strength, i.e., that the system is driven into a more strongly coupled SC regime.

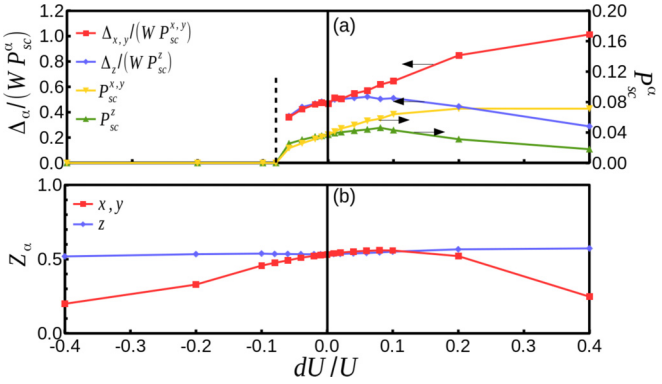

FIG. 9. (a) Orbitally resolved SC order parameter $P_{\rm sc}^{\alpha}$ and ratio $\Delta_\alpha/W P_{\rm sc}^{\alpha}$. (b) Orbitally resolved quasiparticle weight Z_α as a function of interaction imbalance dU/U.

To this aim, it is important to consider the different orbitals separately. In Fig. 9(a) we display the orbitally resolved SC order parameters $P_{\rm sc}^{\alpha}$ as a function of dU/U. As is clear from this figure, the action takes place in the x and y orbitals for which $P_{\rm sc}^{x,y}$ increases to large values with dU/U. In contrast, after a small initial increase $P_{\rm sc}^{z}$ becomes quickly negligible. This corresponds to the dominant pair formation in a resonant state between the x and y orbital, as discussed before.

In order to reveal the effective SC coupling, we consider the dimensionless ratio $\Delta_\alpha/W P_{\rm sc}^{\alpha}$. In a weak-coupling BCS superconductor, $\Delta = P_{\rm sc} V_{\rm at}$, where $V_{\rm at}$ is the effective attractive interaction. Hence, this ratio equals $V_{\rm at}/W$ ($\ll 1$ in the BCS regime) and is a good indicator of the effective dimensionless coupling.

This ratio is also displayed in Fig. 9(a) as a function of dU/U. For $U/W = 1, J_{\rm inv}/W = -0.04$ studied here, we see that it takes a value ∼0.5 in the degenerate case $dU = 0$, indicating already a sizable SC coupling. As dU is increased, this ratio becomes small for the z orbital but increases rapidly for the x, y orbitals, reaching a value of order unity at $dU/U = 0.4$. Hence the system is clearly driven into a strong-coupling SC regime by the interaction imbalance perturbation.

It is interesting to compare and contrast this finding to the effect of uniformly increasing U/W in the degenerate case: $\Delta/W P_{\rm sc}$ is plotted vs U/W for this case in Fig. 10 of Appendix A 1. At small U/W and $|J_{\rm inv}|/W$ (weak-coupling regime), it takes a value close to $2|J_{\rm inv}|/W$, the pairing interaction predicted by BCS mean-field decoupling being $2|J_{\rm inv}|$ at $U = 0$. As U/W is increased, it also increases to values of order unity. However, in this case, the Mott transition is reached at a critical value $(U/W)_c \simeq 2$ at which the quasiparticle weight Z vanishes. In contrast [Fig. 9(b)] strong-coupling superconductivity can be achieved by the imbalance perturbation without $Z_{x,y}$ becoming very small. Since Z enters the superfluid density, we conclude that the interaction imbalance perturbation permits a robust strongly coupled superconductor without being limited by the proximity of the Mott transition.

VI. CONCLUSION AND PERSPECTIVES

Motivated by the recent experimental report of Mitrano *et al.* [39], we have investigated in this article possible

theoretical mechanisms for enhanced superconductivity in A_3C_{60} fullerenes, based on the IHSC model.

Our main finding is that an interaction imbalance corresponding to a smaller value of the Coulomb matrix element for two of the orbitals in comparison to the third one is indeed a perturbation which efficiently enhances SC. We have identified the physical mechanism responsible for this enhancement. It consists of a stabilization of the intramolecular states containing a singlet pair, while preserving the orbital fluctuations associated with the pair-hopping interaction term. These fluctuations allow for the pair to be delocalized coherently between two orbitals. Interaction imbalance was shown to bring SC further into the strong-coupling regime. It provides a distinct and more efficient way to control and enhance SC in these compounds than the volume control corresponding to a uniform change of the bandwidth and interaction strength for all orbitals.

Furthermore, we have performed first-principle calculations of the changes of the electronic structure and of the screened Coulomb matrix elements of K_3C_{60}, associated with the deformation due to the pumped T_{1u} intramolecular mode. Our results demonstrate that indeed an interaction imbalance with a favorable sign and magnitude for SC enhancement is induced by this deformation.

Our work calls for several future studies. The amplitude of the modulation of the T_{1u} mode quoted in Ref. [41] and used in the present work is but an order of magnitude estimate, and a more precise *ab initio* determination is desirable (as well as a direct experimental determination of the transient modulation of the structure). The light excitation may also induce other relevant changes in the material besides the interaction imbalance considered here, such as more complex changes in the band structure, a modulation of the interorbital Coulomb matrix element, and even a direct modulation of the inverted effective Hund's coupling (due, e.g., to an induced displacement and modulation of Jahn-Teller modes). Intermolecular phonons could also be an active part of pairing in the new excited structure [39].

Obviously however, the most pressing extension of our work is to perform a nonequilibrium study in which the changes in electronic structure and orbital-dependent interaction strengths are time dependent. We note in this respect that, as noted in Ref. [41], the dynamical selective excitation of a specific phonon mode leads to a modulation of the Coulomb interaction at twice the frequency of the excited phonon. This is because the electronic density of t_{1u} orbitals have inversion symmetry, implying that the modulation of U couples at lowest order to the square of the phonon collective coordinate $Q^2_{T_{1u}}$. This corresponds to a frequency $\sim$0.4 eV, i.e., a 10 fs time scale, 100 times faster than the picosecond time scales over which the SC state is observed in the experiments of Ref. [39]. Hence, the interaction modulation is in the antiadiabatic limit, providing some justification to the equilibrium treatment performed in the present article. Furthermore, the $Q^2_{T_{1u}}$ coupling also implies that the dU modulation will remain positive during all the cycle, hence leading to a positive time-averaged dU. Nonetheless, a full nonequilibrium treatment is of course needed and will be considered in future work.

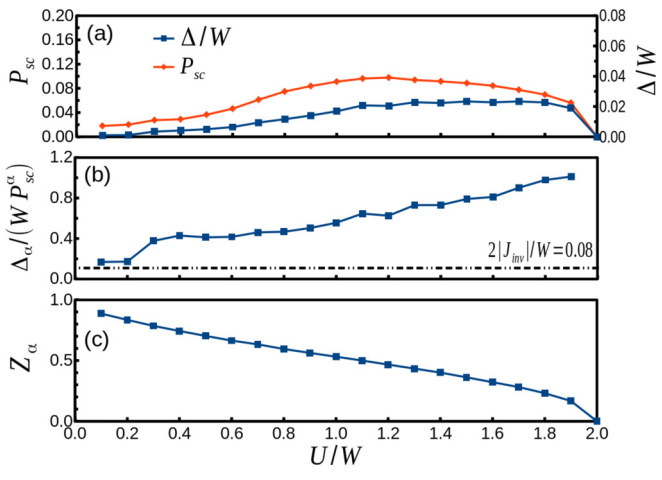

FIG. 10. Degenerate case (three equivalent orbitals). (a) SC order parameter P_{sc}, and gap Δ, as a function of U/W. (b) Ratio between SC gap and order parameter for each orbital $\Delta/W P^{\alpha}_{sc}$. (c) Quasiparticle weight Z as a function of U/W. The dashed-dotted line in (b) denotes the asymptotic value $2|J_{inv}|/W$ of the attractive coupling which holds in the weak-coupling BCS regime $U/W \to 0, |J_{inv}| \ll W$ (see Sec. V C).

ACKNOWLEDGMENTS

We acknowledge useful discussions with Silke Biermann, Massimo Capone, Andrea Cavalleri, Stephen Clark, Dieter Jaksch, Giacomo Mazza, and Alaska Subedi (who also generously shared his calculations of the transient structures). This work was supported by the European Research Council (ERC-319286 QMAC, ERC-617196 CORRELMAT, ERC-278472-MottMetals), and by the Swiss National Science Foundation (NCCR MARVEL).

APPENDIX

1. Superconductivity in the degenerate case

Figure 10 displays P_{sc}, Δ, Δ/P^{α}_{sc}, and the quasiparticle spectral weight Z as a function of U/W in the degenerate case. As discussed in the Sec. V C, the enhancement of U/W in the degenerate case drives the system into a strong-coupling SC regime, as evidenced by the increasing ratio $\Delta/W P^{\alpha}_{sc}$. In contrast to Fig. 9 however, the quasiparticle spectral weight diminishes rapidly as shown in Fig. 10(c), and the enhancement of SC is cut off by entering the Mott phase.

2. Equivalence of positive and negative crystal fields

Figure 11 illustrates the electron-hole symmetry between $h_{CF} > 0$ and $h_{CF} < 0$ cases (see Ref. [47]). As shown in Fig. 11(a), a spin singlet in the electron picture for $h_{CF} > 0$ corresponds to a spin singlet in the hole picture for $h_{CF} < 0$ (red dotted circles). A lone electron for $h_{CF} > 0$ corresponds to a lone hole for $h_{CF} < 0$ as shown in green dotted circles.

From this electron-hole correspondence, P_{sc}, P^{α}_{sc}, and Δ_{α} exhibit symmetric behavior with respect to $h_{CF} = 0$ axis as shown in Fig. 11(b). Also in Fig. 11(c), the orbital occupancy for $h_{CF} > 0$ in the electron picture is symmetric with that for $h_{CF} < 0$ in the hole picture. For positive h_{CF},

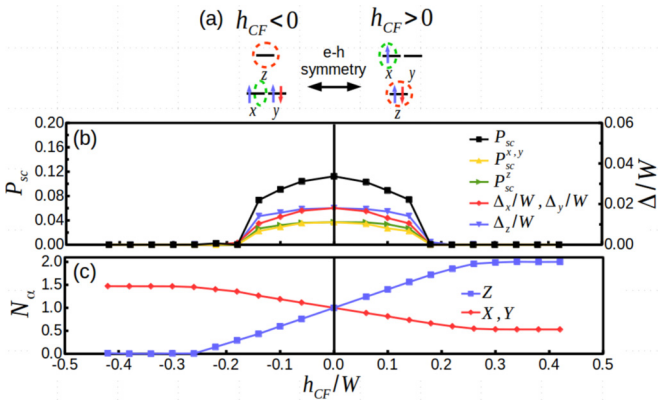

FIG. 11. (a) Electron-hole symmetry in the negative and positive $h_{\rm CF}$ cases. (b) SC order parameter $P_{\rm sc}$, orbitally resolved pairing amplitude $P^{\alpha}_{\rm sc}$, and SC gaps Δ_α/W in the presence of perturbation of Eq. (5) for negative and positive $h_{\rm CF}$ values. (c) Orbital occupancies for negative and positive $h_{\rm CF}$ values.

full orbital polarization occurs around $h_{\rm CF}/W = 0.3$ with orbital occupancies $N_{x,y} = 0.5$ and $N_z = 2$. For negative $h_{\rm CF}$, full orbital polarization occurs around $h_{\rm CF}/W = -0.3$ with orbital occupancies $N_{x,y} = 1.5$ and $N_z = 0$. In the hole picture, these occupancies correspond to 0.5 for x and y, and 2 for z, which is symmetric with positive $h_{\rm CF}/W = 0.3$ case.

3. Spectral function

Figure 12 presents partial density of states (PDOS) of orbitals x, y, and z in the (a) and (b) unperturbed degenerate,

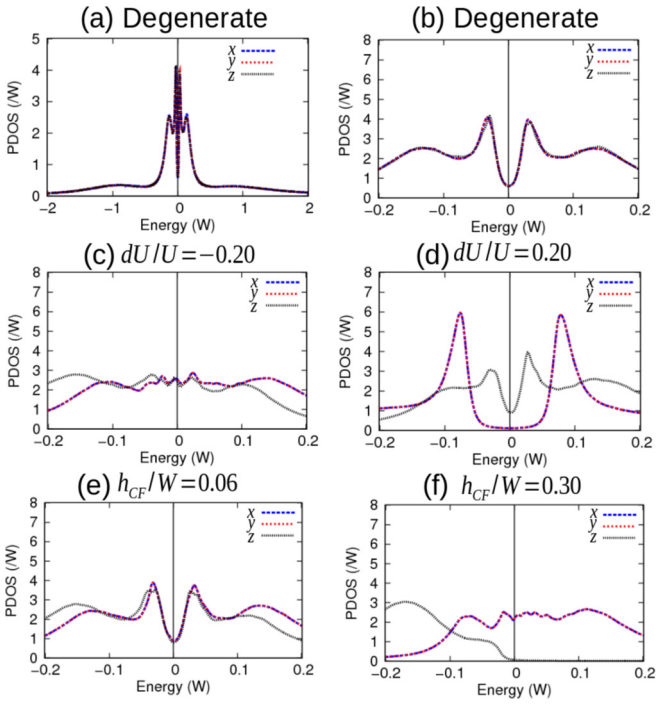

FIG. 12. Partial density of states (PDOS) for orbital x, y, and z in the (a) and (b) degenerate, (c) $dU/U = -0.20$, (d) $dU/U = 0.20$, (e) $h_{\rm CF}/W = 0.06$, and (f) $h_{\rm CF}/W = 0.30$ cases. Lorentzian smearing with the width of $0.004W$ is used in depicting PDOS.

(c) $dU/U = -0.20$, (d) $dU/U = 0.20$, (e) $h_{\rm CF}/W = 0.06$, and (f) $h_{\rm CF}/W = 0.30$ cases.

In the unperturbed case Figs. 12(a) and 12(b) overall PDOS consists of the quasiparticle part, whose width is about $0.5W$, and lower and upper Hubbard bands located at an energy scale of $\sim U = W$. The width of the quasiparticle peak corresponds to the energy scale of Kondo temperature, and agrees well with ZW with the quasiparticle weight Z ($\sim$0.5 for $U/W = 1$). There exists a gap around the Fermi level due to the symmetry breaking into SC phase. The energy scale of the SC gap $\sim 0.04W$ (see Fig. 1, $U/W = 0$) is smaller than that of Kondo temperature. These two energy scales are also discussed in Ref. [3].

In the imbalanced Coulomb interaction with $dU/U = -0.20$ case [Fig. 12(c)], consistent with the results in Fig. 1, SC gaps are completely suppressed for all orbitals without full orbital polarization. All x-, y-, and z-orbital PDOSs cross the Fermi level with up-shifting for x and y orbitals, and down-shifting for the z orbital, respectively. In the $dU/U = 0.20$ case of Fig. 12(d), also consistent with the results in Fig. 1, SC gaps in x and y orbital $\Delta_{x,y}$ are much larger than that of z orbital Δ_z, i.e., SC gaps are anisotropic.

In the crystal-field case with $h_{\rm CF}/W = 0.06$ [Fig. 12(e)], PDOSs of x and y orbitals are shifted up, and that of the z orbital is shifted down. However, SC gaps for all orbitals are resilient, consistent with Fig. 2. The anisotropy in the size of SC gap is small. For a large crystal field, $h_{\rm CF}/W = 0.30$ [Fig. 12(f)], PDOS shows complete orbital polarization. With this complete orbital polarization, SC gaps for all orbital are suppressed, consistent with Fig. 2.

4. *Ab initio* calculations: Methods

In the present study we employ the QUANTUM ESPRESSO package [62,63] to perform *ab initio* calculations for fcc K_3C_{60}. In the band structure calculation, we adopt the generalized-gradient approximation (GGA) with the Perdew-Burke-Ernzerhof parametrization [64] for the exchange-correlation functional. We prepare the Troullier-Martins norm-conserving pseudopotentials [65] in the Kleinman-Bylander representation [66] for the carbon and potassium atoms with the valence configurations $(2s)^{2.0}(2p)^{2.0}$ and $(3p)^{6.0}(4s)^{0.0}(3d)^{0.0}$, respectively. We take into account the nonlinear core correction [67] in the pseudopotential for the potassium atom. The calculation is done with $5 \times 5 \times 5\,\mathbf{k}$ mesh. The cutoff energy for the wave functions is 40 Ry. The calculations of the Coulomb interaction parameters are done within cRPA [56]. The dielectric function is expanded with the plane waves with the energy cutoff of 7.5 Ry. We employ 335 bands (129 occupied + 3 t_{1u} bands + 203 unoccupied) to calculate the polarization function which exclude the transitions within t_{1u} manifold. The generalized tetrahedron method [68,69] was applied to perform the Brillouin-zone integral with respect to the wave vector. We construct maximally localized Wannier functions [70,71] from t_{1u} manifold, and the cRPA interaction parameters are given by the Wannier matrix elements of partially screened Coulomb interactions.

The structures used in the calculation are same as Ref. [39].

(1) fcc K_3C_{60} with the lattice constant 13.89 Å.

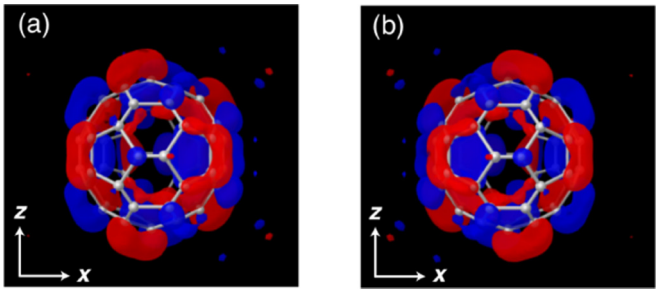

FIG. 13. (a) Bottom-left and (b) bottom-center Wannier functions in Fig. 4 viewed along the y axis. Red (blue) color corresponds to positive (negative) isosurface of the wave function. For visibility, only a single C_{60} molecule in K_3C_{60} solid is shown. In (b), global phase factor (-1) is multiplied to the Wannier function. It is easy to see that these two Wannier functions are related by symmetry, and thus equivalent.

(2) fcc K_3C_{60} ($a = 13.89$ Å) + $T_{1u}(4)$ distortion (amplitude: 2.0 Å$\sqrt{(\text{amu})}$).

(3) fcc K_3C_{60} ($a = 13.89$ Å) + $T_{1u}(4) + H_g(1)$ distortions (amplitudes: 2.0 and 1.5 Å$\sqrt{(\text{amu})}$, respectively).

The obtained cRPA result for K_3C_{60} in equilibrium structure is consistent with the estimate in Ref. [54].

5. Equivalence of p_x-like and p_y-like Wannier functions in Fig. 4 (bottom panel)

Figures 13(a) and 13(b) show the bottom-left and bottom-center Wannier functions in Fig. 4 viewed along the y axis. Here the y axis is the direction of the T_{1u} pumping. We see that these two Wannier functions are related by symmetry, and thus are equivalent.

6. Detailed composition of eigenstates in Fig. 8

Figure 14 presents energy eigenstates in the probability histogram of Fig. 8.

As shown in Fig. 8, for $dU/U = 0.06$, the state which has the highest probability, a3, shows symmetric resonance

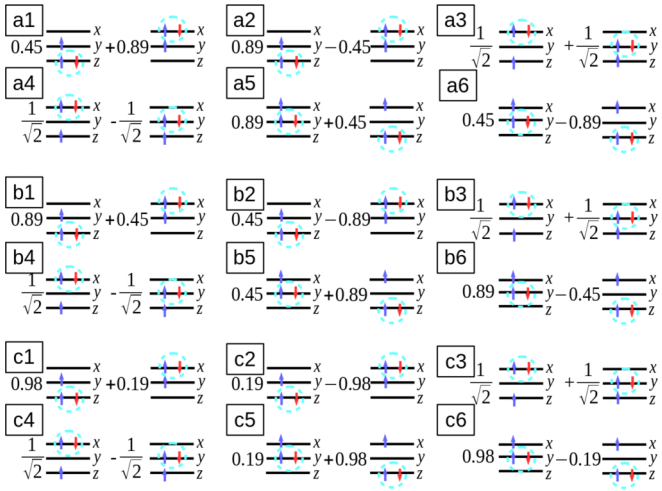

FIG. 14. Energy eigenstates in Fig. 8, a1–a6, b1–b6, and c1–c6.

between states with the spin singlet in x and y orbitals. Also noteworthy is that the probability of asymmetric resonant states between the state with a singlet in the z orbital and the state with a singlet in the x or y orbital, as shown in a1 and a5 states, is larger than that of the $(S = 1/2, L = 1)$ resonant state in the degenerate case. This result implies that the stabilization of a x- and y-orbital singlet also promotes the SC gap in the z orbital Δ_z for $dU/U = 0.06$ which is consistent with Fig. 1(a).

In the case of $dU/U = -0.06$, for states that have the highest probability, b1 and b5, the coefficient for the state with the z-orbital spin singlet (0.89) is much larger than that of the state with the x- or y-orbital singlet (0.45). This suggests that the singlet electron pair is localized mainly in the z orbital. As a result, the orbital fluctuation is suppressed.

Also, in the case of $h_{\text{CF}}/W = 0.10$, for states that have the highest probability, c1 and c5, the coefficient for the state with the z-orbital spin singlet (0.98) is much larger than that for state with the x- or y-orbital spin singlet (0.19). Thus, the singlet pair is localized in the z orbital, suppressing the orbital fluctuation.

[1] A. F. Hebard, M. J. Rosseinsky, R. C. Haddon, D. W. Murphy, S. H. Glarum, T. T. M. Palstra, A. P. Ramirez, and A. R. Kortan, Nature (London) **350**, 600 (1991).

[2] T. Palstra, O. Zhou, Y. Iwasa, P. Sulewski, R. Fleming, and B. Zegarski, Solid State Commun. **93**, 327 (1995).

[3] M. Capone, M. Fabrizio, C. Castellani, and E. Tosatti, Rev. Mod. Phys. **81**, 943 (2009).

[4] O. Gunnarsson, *Alkali-Doped Fullerides: Narrow-Band Solids with Unusual Properties* (World Scientific, Singapore, 2004).

[5] J. E. Han, O. Gunnarsson, and V. H. Crespi, Phys. Rev. Lett. **90**, 167006 (2003).

[6] C. M. Varma, J. Zaanen, and K. Raghavachari, Science **254**, 989 (1991).

[7] M. Schluter, M. Lannoo, M. Needels, G. A. Baraff, and D. Tománek, Phys. Rev. Lett. **68**, 526 (1992).

[8] I. I. Mazin, S. N. Rashkeev, V. P. Antropov, O. Jepsen, A. I. Liechtenstein, and O. K. Andersen, Phys. Rev. B **45**, 5114 (1992).

[9] F. C. Zhang, M. Ogata, and T. M. Rice, Phys. Rev. Lett. **67**, 3452 (1991).

[10] M. J. Rice, H. Y. Choi, and Y. R. Wang, Phys. Rev. B **44**, 10414 (1991).

[11] Y. Asai and Y. Kawaguchi, Phys. Rev. B **46**, 1265 (1992).

[12] S. Suzuki, S. Okada, and K. Nakao, J. Phys. Soc. Jpn. **69**, 2615 (2000).

[13] Y. Takada, J. Phys. Chem. Solids **54**, 1779 (1993).

[14] S. Chakravarty, M. P. Gelfand, and S. Kivelson, Science **254**, 970 (1991).

[15] H.-C. Jiang and S. Kivelson, Phys. Rev. B **93**, 165406 (2016).

[16] M. Capone, M. Fabrizio, and E. Tosatti, Phys. Rev. Lett. **86**, 5361 (2001).

[17] M. Capone, M. Fabrizio, C. Castellani, and E. Tosatti, Science **296**, 2364 (2002).
[18] M. Capone, M. Fabrizio, C. Castellani, and E. Tosatti, Phys. Rev. Lett. **93**, 047001 (2004).
[19] Y. Nomura, S. Sakai, M. Capone, and R. Arita, Sci. Adv. **1**, e1500568 (2015).
[20] Y. Nomura, S. Sakai, M. Capone, and R. Arita, J. Phys.: Condens. Matter **28**, 153001 (2016).
[21] A. Koga and P. Werner, Phys. Rev. B **91**, 085108 (2015).
[22] K. Steiner, S. Hoshino, Y. Nomura, P. Werner, Phys. Rev. B **94**, 075107 (2016).
[23] A. P. Ramirez, M. J. Rosseinsky, D. W. Murphy, and R. C. Haddon, Phys. Rev. Lett. **69**, 1687 (1992).
[24] O. Gunnarsson, Rev. Mod. Phys. **69**, 575 (1997).
[25] A. Y. Ganin, Y. Takabayashi, Y. Z. Khimyak, S. Margadonna, A. Tamai, M. J. Rosseinsky, and K. Prassides, Nat. Mater. **7**, 367 (2008).
[26] Y. Takabayashi, A. Y. Ganin, P. Jeglič, D. Arčon, T. Takano, Y. Iwasa, Y. Ohishi, M. Takata, N. Takeshita, K. Prassides, and M. J. Rosseinsky, Science **323**, 1585 (2009).
[27] A. Y. Ganin, Y. Takabayashi, P. Jeglič, D. Arčon, A. Potočnik, P. J. Baker, Y. Ohishi, M. T. McDonald, M. D. Tzirakis, A. McLennan, G. R. Darling, M. Takata, M. J. Rosseinsky, and K. Prassides, Nature (London) **466**, 221 (2010).
[28] G. Klupp, P. Matus, K. Kamarás, A. Y. Ganin, A. McLennan, M. J. Rosseinsky, Y. Takabayashi, M. T. McDonald, and K. Prassides, Nat. Commun. **3**, 912 (2012).
[29] Y. Kasahara, Y. Takeuchi, T. Itou, R. H. Zadik, Y. Takabayashi, A. Y. Ganin, D. Arčon, M. J. Rosseinsky, K. Prassides, and Y. Iwasa, Phys. Rev. B **90**, 014413 (2014).
[30] A. Potočnik, A. Krajnc, P. Jeglič, Y. Takabayashi, A. Y. Ganin, K. Prassides, M. J. Rosseinsky, and D. Arčon, Sci. Rep. **4**, 4265 (2014).
[31] R. H. Zadik, Y. Takabayashi, G. Klupp, R. H. Colman, A. Y. Ganin, A. Potočnik, P. Jeglič, D. Arčon, P. Matus, K. Kamarás *et al.*, Sci. Adv. **1**, e1500059 (2015).
[32] Y. Ihara, H. Alloul, P. Wzietek, D. Pontiroli, M. Mazzani, and M. Riccò, Phys. Rev. Lett. **104**, 256402 (2010).
[33] Y. Ihara, H. Alloul, P. Wzietek, D. Pontiroli, M. Mazzani, and M. Riccò, Europhys. Lett. **94**, 37007 (2011).
[34] P. Wzietek, T. Mito, H. Alloul, D. Pontiroli, M. Aramini, and M. Riccò, Phys. Rev. Lett. **112**, 066401 (2014).
[35] S. Kawasaki, J. Fukui, T. Motoyama, Y. Suzuki, S. Shibasaki, and G.-Q. Zheng, J. Phys. Soc. Jpn. **82**, 014709 (2013).
[36] R. W. Lof, M. A. van Veenendaal, B. Koopmans, H. T. Jonkman, and G. A. Sawatzky, Phys. Rev. Lett. **68**, 3924 (1992).
[37] S. Chakravarty, S. Khlebnikov, and S. Kivelson, Phys. Rev. Lett. **69**, 212 (1992).
[38] O. Gunnarsson and G. Zwicknagl, Phys. Rev. Lett. **69**, 957 (1992).
[39] M. Mitrano, A. Cantaluppi, D. Nicoletti, S. Kaiser, A. Perucchi, S. Lupi, P. Di Pietro, D. Pontiroli, M. Riccò, S. R. Clark *et al.*, Nature (London) **530**, 461 (2016).
[40] M. Capone, M. Fabrizio, P. Giannozzi, and E. Tosatti, Phys. Rev. B **62**, 7619 (2000).
[41] R. Singla, G. Cotugno, S. Kaiser, M. Först, M. Mitrano, H. Y. Liu, A. Cartella, C. Manzoni, H. Okamoto, T. Hasegawa, S. R. Clark, D. Jaksch, and A. Cavalleri, Phys. Rev. Lett. **115**, 187401 (2015).
[42] C. Grimaldi, L. Pietronero, and S. Strässler, Phys. Rev. Lett. **75**, 1158 (1995).
[43] A. Georges, L. de' Medici, and J. Mravlje, Annu. Rev. Condens. Matter Phys. **4**, 137 (2013).
[44] W. F. Brinkman and T. M. Rice, Phys. Rev. B **2**, 4302 (1970).
[45] K. Prassides, S. Margadonna, D. Arcon, A. Lappas, H. Shimoda, and Y. Iwasa, J. Am. Chem. Soc. **121**, 11227 (1999).
[46] V. Brouet, H. Alloul, S. Garaj, and L. Forró, Phys. Rev. B **66**, 155122 (2002).
[47] S. Hoshino and P. Werner, Phys. Rev. B **93**, 155161 (2016).
[48] A. Georges, G. Kotliar, W. Krauth, and M. J. Rozenberg, Rev. Mod. Phys. **68**, 13 (1996).
[49] E. Gull, A. J. Millis, A. I. Lichtenstein, A. N. Rubtsov, M. Troyer, and P. Werner, Rev. Mod. Phys. **83**, 349 (2011).
[50] O. Parcollet, M. Ferrero, T. Ayral, H. Hafermann, I. Krivenko, L. Messio, and P. Seth, Comput. Phys. Commun. **196**, 398 (2015).
[51] P. Seth, I. Krivenko, M. Ferrero, and O. Parcollet, Comput. Phys. Commun. **200**, 274 (2016).
[52] K. Steiner, Y. Nomura, and P. Werner, Phys. Rev. B **92**, 115123 (2015).
[53] P. Sémon, G. Sordi, and A.-M. S. Tremblay, Phys. Rev. B **89**, 165113 (2014).
[54] Y. Nomura, K. Nakamura, and R. Arita, Phys. Rev. B **85**, 155452 (2012).
[55] Y. Nomura and R. Arita, Phys. Rev. B **92**, 245108 (2015).
[56] F. Aryasetiawan, M. Imada, A. Georges, G. Kotliar, S. Biermann, and A. I. Lichtenstein, Phys. Rev. B **70**, 195104 (2004).
[57] M. Först, C. Manzoni, S. Kaiser, Y. Tomioka, Y. Tokura, R. Merlin, and A. Cavalleri, Nat. Phys. **7**, 854 (2011).
[58] A. Subedi, A. Cavalleri, and A. Georges, Phys. Rev. B **89**, 220301 (2014).
[59] H. Suhl, B. Matthias, and L. Walker, Phys. Rev. Lett. **3**, 552 (1959).
[60] J. Kondo, Prog. Theor. Phys. **29**, 1 (1963).
[61] K. Haule, Phys. Rev. B **75**, 155113 (2007).
[62] P. Giannozzi, S. Baroni, N. Bonini, M. Calandra, R. Car, C. Cavazzoni, D. Ceresoli, G. L. Chiarotti, M. Cococcioni, I. Dabo, A. D. Corso, S. de Gironcoli, S. Fabris, G. Fratesi, R. Gebauer, U. Gerstmann, C. Gougoussis, A. Kokalj, M. Lazzeri, L. Martin-Samos, N. Marzari, F. Mauri, R. Mazzarello, S. Paolini, A. Pasquarello, L. Paulatto, C. Sbraccia, S. Scandolo, G. Sclauzero, A. P. Seitsonen, A. Smogunov, P. Umari, and R. M. Wentzcovitch, J. Phys.: Condens. Matter **21**, 395502 (2009).
[63] http://www.quantum-espresso.org/.
[64] J. P. Perdew, K. Burke, and M. Ernzerhof, Phys. Rev. Lett. **77**, 3865 (1996).
[65] N. Troullier and J. L. Martins, Phys. Rev. B **43**, 1993 (1991).
[66] L. Kleinman and D. M. Bylander, Phys. Rev. Lett. **48**, 1425 (1982).
[67] S. G. Louie, S. Froyen, and M. L. Cohen, Phys. Rev. B **26**, 1738 (1982).
[68] T. Fujiwara, S. Yamamoto, and Y. Ishii, J. Phys. Soc. Jpn. **72**, 777 (2003).
[69] Y. Nohara, S. Yamamoto, and T. Fujiwara, Phys. Rev. B **79**, 195110 (2009).
[70] N. Marzari and D. Vanderbilt, Phys. Rev. B **56**, 12847 (1997).
[71] I. Souza, N. Marzari, and D. Vanderbilt, Phys. Rev. B **65**, 035109 (2001).